

Nontrivial Fermi surface topology in kagome superconductor $CsTi_3Bi_5$ revealed by de Haas–van Alphen oscillation

Yuhang Zhang(张宇航), Xinwei Yi(易鑫伟), Zhen Zhao(赵振), Jiali Liu(刘家利), Aini Xu(胥艾妮), Dong Li(李栋), Zouyouwei Lu(鲁邹有为), Yue Liu(刘樾), Jihu Lu(卢佶虎), Hua Zhang(张华), Hui Chen(陈辉), Shiliang Li(李世亮), Ziyi Liu(刘子儀), Jinguang Cheng(程金光), Gang Su(苏刚), Haitao Yang(杨海涛), Xiaoli Dong(董晓莉), Hong-Jun Gao(高鸿钧), and Zhongxian Zhao(赵忠贤)

Citation: Chin. Phys. B, 2025, 34 (**7**): 077107. DOI: 10.1088/1674-1056/adc7f0
http://cpb.iphy.ac.cn; http://iopscience.iop.org/cpb

What follows is a list of articles you may be interested in

Quantum oscillations and nontrivial topology in unfilled skutterudite $IrSb_3$

Yang Yang(杨扬), Xinyao Li(李鑫垚), Feihong Guan(关飞鸿), Majeed Ur Rehman, Wei Ning(宁伟), Xiangde Zhu(朱相德), and Mingliang Tian(田明亮)

Chin. Phys. B, 2025, 34 (**6**): 067103. DOI: 10.1088/1674-1056/adc7f2

The de Haas-van Alphen quantum oscillations in the kagome metal $RbTi_3Bi_5$

Zixian Dong(董自仙), Lei Shi(石磊), Bin Wang(王彬), Mengwu Huo(霍梦五), Xing Huang(黄星), Chaoxin Huang(黄潮欣), Peiyue Ma(马培跃), Yunwei Zhang(张云蔚), Bing Shen(沈冰), and Meng Wang(王猛)

Chin. Phys. B, 2024, 33 (**10**): 107102. DOI: 10.1088/1674-1056/ad6a0a

Two-dimensional Sb net generated nontrivial topological states in $SmAgSb_2$ probed by quantum oscillations

Jian Yuan(袁健), Xian-Biao Shi(石贤彪), Hong Du(杜红), Tian Li(李田), Chuan-Ying Xi(郗传英), Xia Wang(王霞), Wei Xia(夏威), Bao-Tian Wang(王保田), Rui-Dan Zhong(钟瑞丹), and Yan-Feng Guo(郭艳峰)

Chin. Phys. B, 2024, 33 (**7**): 077102. DOI: 10.1088/1674-1056/ad4bc2

In-plane uniaxial-strain tuning of superconductivity and charge-density wave in CsV_3Sb_5

Xiaoran Yang(杨晓冉), Qi Tang(唐绮), Qiuyun Zhou(周秋韵), Huaiping Wang(王怀平), Yi Li(李意), Xue Fu(付雪), Jiawen Zhang(张加文), Yu Song(宋宇), Huiqiu Yuan(袁辉球), Pengcheng Dai(戴鹏程), and Xingye Lu(鲁兴业)

Chin. Phys. B, 2023, 32 (**12**): 127101. DOI: 10.1088/1674-1056/acf707

Tri-hexagonal charge order in kagome metal CsV_3Sb_5 revealed by ^{121}Sb nuclear quadrupole resonance

Chao Mu(牟超), Qiangwei Yin(殷蔷薇), Zhijun Tu(涂志俊), Chunsheng Gong(龚春生), Ping Zheng(郑萍), Hechang Lei(雷和畅), Zheng Li(李政), and Jianlin Luo(雒建林)

Chin. Phys. B, 2022, 31 (**1**): 017105. DOI: 10.1088/1674-1056/ac422c

---

SPECIAL TOPIC — Recent progress on kagome metals and superconductors

Nontrivial Fermi surface topology in kagome superconductor $CsTi_3Bi_5$ revealed by de Haas–van Alphen oscillation

Yuhang Zhang(张宇航)[1,2,†,‡], Xinwei Yi(易鑫伟)[2,†], Zhen Zhao(赵振)[1,2,†], Jiali Liu(刘家利)[1,2], Aini Xu(胥艾妮)[1,2], Dong Li(李栋)[6], Zouyouwei Lu(鲁邹有为)[1,2], Yue Liu(刘樾)[1,2], Jihu Lu(卢佶虎)[1,2], Hua Zhang(张华)[1,2], Hui Chen(陈辉)[1,2,4], Shiliang Li(李世亮)[1,2,3], Ziyi Liu(刘子儀)[1], Jinguang Cheng(程金光)[1,2], Gang Su(苏刚)[2,5,7,§], Haitao Yang(杨海涛)[1,2,4,¶], Xiaoli Dong(董晓莉)[1,2,3,♯], Hong-Jun Gao(高鸿钧)[1,2,4], and Zhongxian Zhao(赵忠贤)[1,2,3]

[1] *Beijing National Laboratory for Condensed Matter Physics and Institute of Physics, Chinese Academy of Sciences, Beijing* 100190, *China*
[2] *University of Chinese Academy of Sciences, Beijing* 100049, *China*
[3] *Songshan Lake Materials Laboratory, Dongguan, Guangdong* 523808, *China*
[4] *CAS Center for Excellence in Topological Quantum Computation, University of Chinese Academy of Sciences, Beijing* 100190, *China*
[5] *Kavli Institute for Theoretical Sciences, CAS Center for Excellence in Topological Quantum Computation, University of Chinese Academy of Sciences, Beijing* 100190, *China*
[6] *RIKEN Center for Emergent Matter Science (CEMS), Wako* 351-0198, *Japan*
[7] *CAS Key Laboratory of Theoretical Physics, Institute of Theoretical Physics, Chinese Academy of Sciences, Beijing* 100190, *China*

(Received 22 January 2025; revised manuscript received 29 March 2025; accepted manuscript online 2 April 2025)

The kagome lattice, naturally encompassing Dirac fermions, flat bands, and van Hove singularities, tends to intertwine exotic electronic states. Revealing the characteristics of its Fermi surface will help clarify the nature of the complex quantum phenomena in kagome material. Here we report the Fermi surface properties of the novel kagome metal $CsTi_3Bi_5$ by the de Haas–van Alphen oscillations. The observed oscillations are clear and consist of six principal frequencies ranging from 214 T to 1013 T. The angular dependence of the frequency implies a quasi-two-dimensional electronic structure. In addition, the geometry phase corresponding to 281 T, determined by direct Lifshitz–Kosevich formula fitting, yields a value close to π, which may indicate a band structure with nontrivial topological property. These results underscore the potential of $CsTi_3Bi_5$ as a promising platform to explore the interplay between topological order, electronic nematicity, and superconductivity.

Keywords: kagome superconductor, quantum oscillation

PACS: 71.18.+y, 74.70.–b, 74.25.–q

DOI: 10.1088/1674-1056/adc7f0 **CSTR:** 32038.14.CPB.adc7f0

1. Introduction

The kagome lattice hosts a variety of exotic properties such as geometric frustration, flat bands, van Hove singularities, and Dirac fermions.[1] The quantum interactions between geometry, topology, spin and correlation make this structure more interesting.[2–4] In the Z_2 kagome superconductor AV_3Sb_5 family,[5,6] the intertwining of multiple electronic orders makes the physics interesting and rich. The properties of this system such as unconventional charge density waves,[7–10] superconductivity,[6,11–14] pair density waves,[7] giant anomalous Hall effect,[15,16] time-reversal symmetry breaking,[17,18] and electronic nematic order[7,11,19–21] have attracted much research and controversy.

Recently in a study conducted by some of the authors, a novel Z_2 kagome metal $CsTi_3Bi_5$ system, which shares the same crystal structure as AV_3Sb_5, was discovered to exhibit orbital selective nematic order and possible superconductivity, while no charge density wave (CDW) transition was observed.[22–29] Comparing the similarities and differences between $CsTi_3Bi_5$ and AV_3Sb_5 would contribute to understanding the physics in AV_3Sb_5.

The nonlinear magnetic field dependence of Hall effect in $CsTi_3Bi_5$ below about 70 K points to a similar multiband nature as in CsV_3Sb_5.[26] The van Hove singularity (vHS) in $CsTi_3Bi_5$ can be tuned in a large energy range without structural instability, different from that in CsV_3Sb_5.[27] High resolution laser-based ARPES observes multiple nontrivial band structures such as Dirac nodal loops and nodal lines and nontrivial topological surface states.[23] Further understanding of the details of the three-dimensional (3D) Fermi surface structure of $CsTi_3Bi_5$ is needed. As a crucial method for mapping

†These authors contributed equally to this work.
‡Corresponding author. E-mail: yuhang@iphy.ac.cn
§Corresponding author. E-mail: gsu@ucas.ac.cn
¶Corresponding author. E-mail: htyang@iphy.ac.cn
♯Corresponding author. E-mail: dong@iphy.ac.cn

© 2025 Chinese Physical Society and IOP Publishing Ltd. All rights, including for text and data mining, AI training, and similar technologies, are reserved.

the Fermi surface properties and its topology, the quantum oscillations study for $CsTi_3Bi_5$ is still scarce, which should provide complementary bulk-sensitive insights into Fermi surface topology, and directly quantifying key parameters like effective mass, mean free path, and Berry phase. Previous Shubnikov–de Haas (SdH) oscillation study reported on $RbTi_3Bi_5$ was limited probably by the sample sensitivity.[24] Therefore, a systematic study of the Fermi surface by quantum oscillation on high quality samples is needed.

In this paper, we report a systematic de Haas–van Alpen (dHvA) oscillation study on Fermi surface properties and band topology in $CsTi_3Bi_5$. We obtained six distinct frequencies based on high quality data. The angle dependence of oscillation frequency was found to be well explained by a quasi-two-dimensional (2D) electronic structure. The effective masses and mean free paths corresponding to the different frequencies were obtained by analyzing the amplitude of the oscillations, which are comparable with those of the CsV_3Sb_5.[30–35] Relatively small cyclotron masses m^*, high mobility and nonzero Berry phases provide direct evidence for the existence of nontrivial topological electronic structures in $CsTi_3Bi_5$.

2. Results and discussion

Figure 1(a) shows the magnetization behavior of high-quality single crystal $CsTi_3Bi_5$ under the magnetic field up to 7 T, with the field applied along the c-axis ($\theta = 0°$). In the low field regime, a distinct superconducting diamagnetic signal is observed, while pronounced oscillations become noticeable at field strengths above ~ 3 T. The presence of smooth and intricate oscillations at such a low magnetic field reveals the sample's purity and homogeneity, further attesting to the high quality of the samples.[23] Figure 1(b) presents the polynomial background subtracted oscillations at different temperatures. The magnetization exhibits a well-defined periodicity with respect to $1/B$, which is characteristic of the dHvA oscillation. The amplitude of the oscillation gradually diminishes with increasing temperature and disappears completely around 12 K. The oscillation apparently contains multiple frequencies, implying a complex Fermi surface structure.

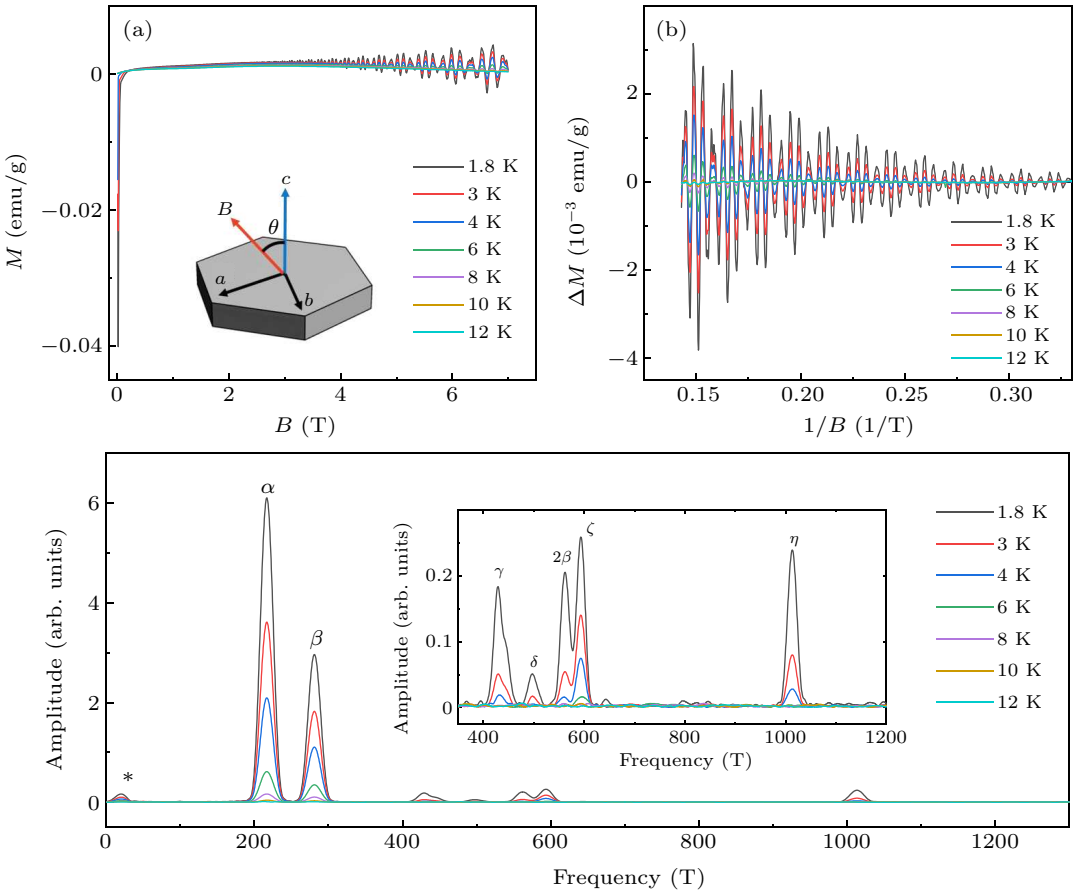


Fig. 1. Temperature dependence and FT of dHvA oscillations in $CsTi_3Bi_5$. (a) Field dependent magnetization of $CsTi_3Bi_5$. The superconductivity is clear in low field and well-defined dHvA oscillations occur in higher field. (b) Oscillations after subtracting background from (a). The amplitude decreases with the increase of temperature, and finally fades at ~ 12 K. (c) FT of (b), showing three peaks in the low frequencies and five recognizable peaks in the higher frequencies (inset).

Here we use discrete-time Fourier transform to refine the spectrum in order to obtain more precise frequencies (F) and amplitude values. As shown in Fig. 1(c), the Fourier transform spectrum of the oscillations in Fig. 1(b) displays six fundamental frequencies and one harmonic frequency, denoted by $F_\alpha = 217$ T, $F_\beta = 281$ T, $F_\gamma = 429$ T, $F_\delta = 498$ T, $F_\zeta = 594$ T,

$F_\eta = 1013$ T and $F_{2\beta} = 562$ T. Note that there are several small peaks in Fig. 1(c), such as the lowest frequency ($F = 12$ T) which is most likely caused by extrinsic effects from data processing (e.g., background subtraction and Fourier transform). The frequency of quantum oscillations can be described by the Onsager's relation[27] $F = (\hbar/2\pi e)A_F$, where A_F is the extremal cross-sectional area in Fermi surface perpendicular to the magnetic field direction. Therefore, the presence of six frequencies implies that there are six Fermi wave vectors each corresponding to one frequency and that $CsTi_3Bi_5$ has complex Fermi surfaces with several pockets. In addition, the magnetization oscillation amplitude could be explained by the Lifshitz–Kosevich (LK) formula[36,37] with Berry phase being taken into account

$$\Delta M \propto -\sqrt{B}\sum_i \sum_{r=1}^{\infty} r^{-3/2} R_T^{i,r} R_D^{i,r} \sin\left[2\pi r\left(\frac{F^i}{B} - \frac{1}{2} + \varphi^i\right)\right].$$

The magnetization oscillation is proportional to a linear superposition of sine functions from different orbitals (i) and their harmonics (r). The phase factor φ stands for the geometry phase, generally pointing to the Berry phase, which is close to 0.5 for a topologically nontrivial band, and 0 for a trivial band.[38] The decay term $R_T = (\alpha m^* T/\mu_0 B)/\sinh(\alpha m^* T/\mu_0 B)$ and $R_D = \exp(-\alpha m^* T_D/\mu_0 B)$ come from temperature and scattering. Here, $\alpha \approx 14.69$ T/K is a constant. m^* is the cyclotron effective mass in units of free electron mass m_e. $T_D = \hbar/(2\pi k_B \tau_q)$, where τ_q is quantum scattering time.

Therefore, the effective mass m^* and the quantum scattering time can be obtained by fitting the temperature dependence of the amplitude of each oscillation frequency. Since there are multiple frequencies in the $CsTi_3Bi_5$ oscillation data, it is difficult to directly determine the amplitude corresponding to each frequency. To estimate m^*, a common approach is taking the Fourier transform amplitude instead of the original amplitude, and taking the harmonic average magnetic field within Fourier transform window. The best fitting of effective mass for F_α, F_β and F_ζ is shown in Fig. 2(a), and the fitting for γ, δ, and η-orbit is shown in Fig. S2(a). Similarly, by performing Fourier transform on oscillations with shifting magnetic field windows and replacing the magnetic field with the harmonic average of the magnetic field from the FT window, the magnetic field dependence of the oscillation amplitude of each orbit can be obtained. Then, the standard Dingle plot procedure can be applied, or the damping of oscillation can be directly fitted using $R_D = \exp\left(-\alpha m^* \hbar/(2\pi k_B \tau_q \mu_0 B)\right)$, as shown in Fig. 2(b) (F_α, F_β and F_ζ) and S2(b) (F_γ, F_δ, and F_η). The mean free path l_q and the quantum mobility μ_q are obtained thereafter. The estimated values of Fermi surface parameters for each orbit are presented in Table 1. The determined m^* of $CsTi_3Bi_5$ is small and comparable with that reported in CsV_3Sb_5,[30–35] which is usually correlated to Dirac modes. Unlike m^*, the mean free path is obviously larger than that in CsV_3Sb_5,[30–35] which makes a quite high quantum mobility. μ_q is even ten times larger than the classical mobility μ_c from Hall effect.[26] This difference in the two mobilities may be due to the sample's quality. The RRR of the sample used in this work is around 63 (Fig. S4), which is much higher than reported. Additionally, this may also be due to the fact that these two scattering times represent different scattering processes.[39]

Table 1. Fermi surface parameters from oscillations. F, A_F, m^*, m_e, τ_q, l_q, μ_q stand for frequency, cross-sectional area on the Fermi surface, effective mass/free electron mass, quantum scattering time, mean free path, quantum mobility, respectively.

	F (T)	A_F (Å^{-2})	m^*/m_e	τ_s (10^{-13} s)	l_q (nm)	μ_q (m^2·V^{-1}·s^{-1})
α	217	0.0207	0.29	43.5	1409	2.63
β	281	0.0268	0.27	36.6	1449	2.38
γ	429	0.0409	0.51	21.5	556	0.74
δ	498	0.0475	0.47	42.7	1294	1.59
ζ	594	0.0566	0.32	24.7	1200	1.36
η	1013	0.0966	0.47	24.8	1069	0.93

Some of these Fermi surfaces have nontrivial topological properties based on theoretical calculations and previous ARPES experiments.[25,27,28] The standard method for studying its topological nature is to construct Landau level fan diagrams. After using filters to isolate a given frequency, Landau levels are labeled corresponding to $N + 1/4$ for maxima, and $N - 1/4$ at minima, and N represents the integer Landau level index. However, the maximum magnetic field applied is 7 T, which means the minimum integer Landau level index from the oscillation for F_α and F_β is around 30. In such a situation, there may be a considerable error in the conclusion from a typical LL fan plot. Especially in a multiband system, additional errors could come out in the preposed FFT filtering procedure due to the selection of intervals. Thus, we carefully verified the results under different linear fitting ranges (Fig. S3), indicating that the reliability of LL fan plot results is not high enough under these conditions.

Therefore, a direct LK formula fitting procedure is adopted. It is convenient to set only the frequency and phase factor as fitting arguments based on the parameters obtained from the previous fits, which makes this fitting procedure highly sensitive to the phase factor. And since the amplitude of the low frequency components is much larger than that of the high frequency components, only F_α and F_β and their harmonic components were considered in the fit in order to reduce the uncertainty caused by more parameters. As shown in Fig. 2(c), the fitting results are very close to the experimental data, illustrating the reasonableness of the fitting parameters and the procedure. Since these orbits exhibit relatively low frequencies, our measurement range already captured sufficient oscillation periods for robust analysis. Based on our systematic approach and the quality of the data, we believe

the phase factor determination for these orbits is quite reliable. The phase factor corresponding to the best fit is 0.02 and 0.41 for F_α and F_β. The phase factor of F_β is close to the predicted $\varphi_B \sim 0.5$ for topological orbits, which may imply a Berry phase close to π.

To further investigate the anisotropic electronic structure of $CsTi_3Bi_5$, we measured the magnetization in selected angles θ and applied Fourier transform analysis, as shown in Figs. 3(a) and 3(b). The amplitude of oscillations is decreased with increasing θ, and there is no oscillation observed above $\theta = 60°$, which is a character of the cylindrical Fermi surface. The frequencies increase with θ. As shown in Fig. 3(c), the angle dependence $F(\theta)$ can be well described by a cylindrical Fermi surface with $F_0/\cos(\theta)$, which is consistent with the theoretical prediction.

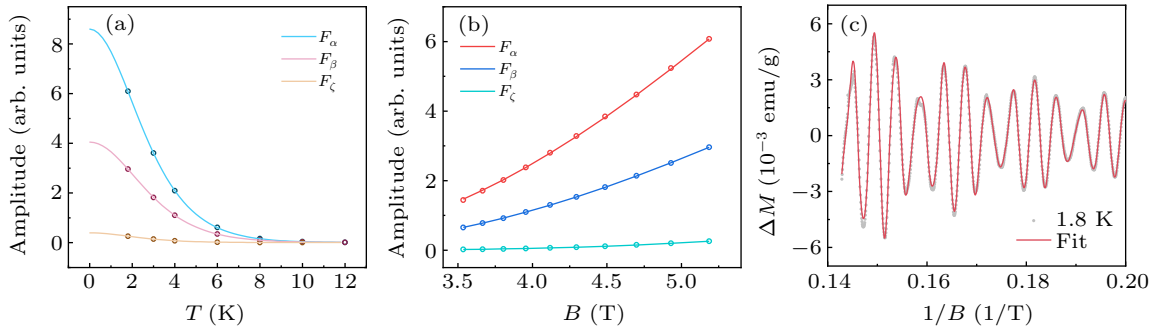


Fig. 2. Analysis of oscillations with LK formula. (a) Temperature dependence of amplitude. The solid line shows the best LK fitting results. The corresponding effective masses are displayed in Table 1. (b) Field dependence of amplitude. The field here is the harmonic average of FFT interval. The solid line shows the best LK fitting results. The fitted mean free path can be found in Table 1. (c) Direct LK formula fitting. The phase factor corresponding to the best fit is 0.02 and 0.41 for F_α and F_β, respectively.

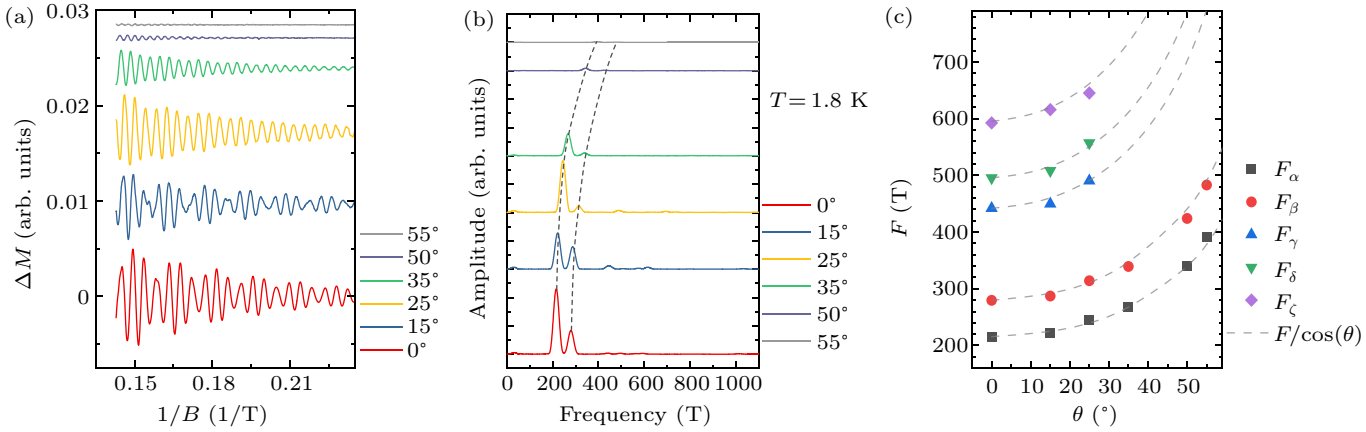


Fig. 3. Angular dependence of oscillations. (a) Oscillations measured at various angles. The amplitude of oscillation decreases rapidly with increasing angle above 50°. (b) Fourier transform of (a). The dash line shows the angle dependence of F_α and F_β. (c) The angle dependence of frequency for each orbit. $F(\theta)$ can be well described by a cylindrical Fermi surface with $F_0/\cos(\theta)$, which presents a quasi-two-dimensional nature of the electronic structure of the system.

Subsequently, the numerical calculations of the extremal cross area on the Fermi surface based on density functional theory (DFT) were carried out to further understand the Fermiology getting from the dHvA oscillation experiments. All Fermi surface pockets display clear 2D features. The Γ-centered circular pocket (colored in red) originates from Bi-p_z orbits, and the remaining ones are mainly contributed by Ti-d orbits. Features of the Fermi surface in Fig. 4(a) have already been experimentally confirmed by quasiparticle interference and ARPES results.[23,28] The quantum oscillation frequencies are directly proportional to A_F as expressed in the equation of Onsager's relation. In Fig. 4(c) of side views of Fermi surface, the cross-sectional area of these Fermi surface pockets reaches the maximum or minimum at $k_c = 0$ or $k_c = \pi/c$ slices, respectively. This means that all extremal orbits are located in either $k_c = 0$ or π/c slices when B is along the c-axis. We concentrate on those closed orbits in $k_c = 0$ and π/c slices with corresponding oscillation frequencies less than the experimental measurement limit of about 1400 T. Six orbitals with oscillation frequencies in the range of 367–723 T at Fermi level $E_{F,exp}$ determined by the ARPES experiment[28] are identified and labeled as F_1–F_6 in Fig. 4(b). A well-defined Fermi level is necessary to determine the orbits accurately. Therefore, an exhaustive search for all oscillation frequencies is performed within a range of $E - E_{F,exp} = \pm 0.15$ eV as plotted in Fig. 4(e). Experimental oscillation frequencies $F_{\alpha-\eta}$ are qualitatively consistent with DFT calculations and each of them intersects several orbits (Fig. 4(e)). When taking the experimental values

$E = E_{\mathrm{F,exp}}$, three frequencies are close to the calculated values. Different from CsV_3Sb_5 with CDW, both experimental measurements and phonon spectrum calculations show the absence of CDW order and Fermi surface distortion in $CsTi_3Bi_5$.[26] Though the number of peaks is less than that in CsV_3Sb_5, which may come from interlayer coupling,[31] there is no singular choice of E_F that can match all experimental frequencies. The quantitatively numerical disagreements between quantum oscillation frequencies and DFT-derived results may imply the complexity of electronic structures of $CsTi_3Bi_5$. Moreover, given its high structural symmetry and strong spin–orbit coupling (SOC), this kagome metal is anticipated to exhibit abundant topological properties in its electronic structures, which again demonstrates the non-trivial topology of $CsTi_3Bi_5$.

In conclusion, through dHvA oscillation analysis, we have identified multiple frequencies with small effective masses in the $CsTi_3Bi_5$ system. Several parameters related to the Fermi surface of $CsTi_3Bi_5$ were obtained by fitting the oscillation pattern with the LK formula. The effective masses of $CsTi_3Bi_5$ are in the range of $0.27m_e$–$0.54m_e$, which are comparable to that of CsV_3Sb_5. The angle-dependent oscillations imply a quasi-2D electronic structure. In addition, we find that the frequency F_β may be related to a non-zero Berry phase, which implies the nontrivial topological properties in $CsTi_3Bi_5$. Hence, the discovery of these properties in $CsTi_3Bi_5$ establishes it as a promising avenue for exploring the interplay between different ordered states in topological materials.

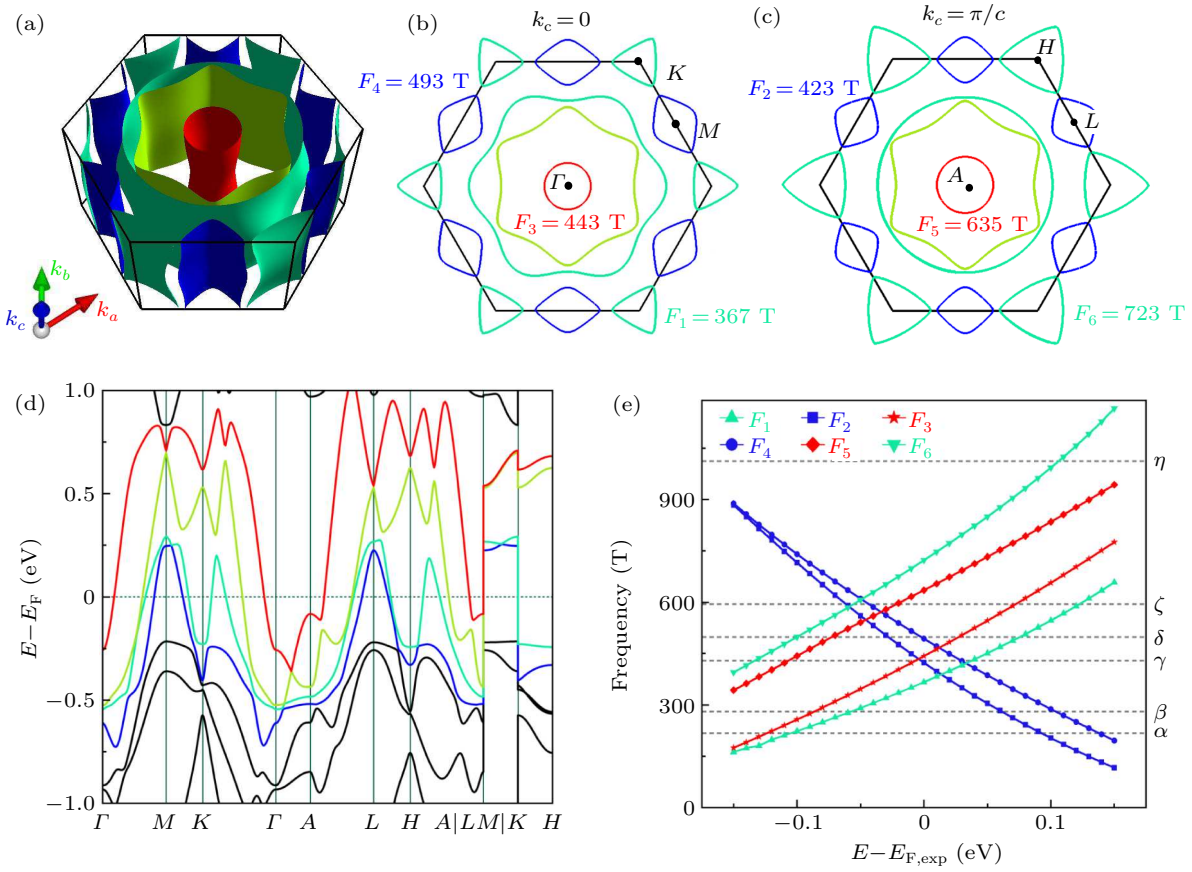


Fig. 4. DFT calculations of Fermi surface and frequencies. (a) Calculated 3D Fermi surface of $CsTi_3Bi_5$ based on the DFT calculations. All Fermi surface pockets display clear 2D features. (b) and (c) 2D maps of Fermi surface and the frequencies at $E = E_{\mathrm{F,exp}}$ related to each orbit at $k_c = 0$ and $k_c = \pi/c$ slices. (d) Calculated band structure of $CsTi_3Bi_5$. (e) The calculated frequencies as a function of Fermi energy. The dashed lines show the frequencies from the oscillation experiment.

Appendix A: Methods

A1. Single crystals preparation and characterization

$CsTi_3Bi_5$ single crystals were grown using a modified self-flux method.[23] The crystal characterization was applied by x-ray diffraction (XRD) at room temperature on a diffractometer (Rigaku SmartLab, 9 kW) equipped with two Ge (220) monochromators. The quality and orientations of the crystals were determined by a Photonic Science vertical Laue crystal orientation system.

A2. Magnetization measurement

The magnetic property measurements were conducted on a MPMS-3 system down to 1.8 K. Residual magnetic fields were eliminated before each measurement to ensure the accuracy. A home-made sample holder with rotation ability was used in the dHvA oscillation measurements.

A3. Calculation details

The implementation of first-principles calculations based on density functional theory (DFT) employs the Vienna *ab initio* simulation package (VASP).[40] All calculations utilize the projector augmented-wave pseudopotential method[41] and the exchange–correlation energy of Perdew–Burke–Ernzerhof parameterization of the generalized gradient approximation (GGA).[42] To ensure the accuracy of our structural optimization, the convergence criterion of atomic forces is set to be less than 10^{-3} eV/Å in VASP. To be consistent with experimental results, we fix the lattice parameters of $CsTi_3Bi_5$ as experimentally measured values of $a = b = 5.76$ Å and $c = 9.49$ Å.[23] In addition, a plane-wave cutoff energy value of 520 eV and a total energy convergence threshold of 10^{-6} eV/atom are set in all calculations. The self-consistent cycles use a Γ centered $20 \times 20 \times 12$ Monkhorst–Pack k-space point grid.

The Fermi surface is interpolated within k-space points of $101 \times 101 \times 101$ based tight-binding model after DFT calculation in order to get a highly precise Fermi surface. Wannier90 package[43] is used in fitting Wannier functions and building tight-binding models. Atomic orbits of Cs-s, Ti-d, and Bi-p participate as guiding projections. Based on the calculated Fermi surface, the angular dependence of extremal orbits, oscillation frequencies and effective electronic mass are calculated using the SKEAF program.[44]

Acknowledgments

We thank professor Ziqiang Wang and Aris Alexandradinata for valuable discussions and suggestions.

Project supported by the National Key Research and Development Program of China (Grant Nos. 2022YFA1403903, 2023YFA1406100, 2018YFA0305800, and 2022YFA1204100), the National Natural Science Foundation of China (Grant Nos. 12304075, 11834014, 61888102, and 12447101), Chinese Academy of Sciences (Grant Nos. XDB33010200 and 2022YSBR-048), the Strategic Priority Research Program of the Chinese Academy of Sciences (Grant No. XDB28000000), and the National Science and Technology Major Project (Grant No. 2024ZD0300500).

References

[1] Syozi I 1951 *Prog. Theor. Phys.* **6** 306
[2] Anderson P W 1973 *Mater. Res. Bull.* **8** 153
[3] Broholm C, Cava R J, Kivelson S A, Nocera D G, Norman M R and Senthil T 2020 *Science* **367** 263
[4] Yin J X, Lian B and Hasan M Z 2022 *Nature* **612** 647
[5] Ortiz B R, Gomes L C, Morey J R, Winiarski M, Bordelon M, Mangum J S, Oswald L W H, Rodriguez-Rivera J A, Neilson J R, Wilson S D, Ertekin E, McQueen T M and Toberer E S 2019 *Phys. Rev. Mater.* **3** 094407
[6] Ortiz B R, Teicher S M L, Hu Y, Zuo J L, Sarte P M, Schueller E C, Abeykoon A M M, Krogstad M J, Rosenkranz S, Osborn R, Seshadri R, Balents L, He J F and Wilson S D 2020 *Phys. Rev. Lett.* **125** 247002
[7] Chen H, Yang H T, Hu B,*et al.* 2021 *Nature* **599** 222
[8] Jiang Y X, Yin J X, Denner M M,*et al.* 2021 *Nat. Mater.* **20** 1353
[9] Liang Z W, Hou X Y, Zhang F, Ma W R, Wu P, Zhang Z Y, Yu F H, Ying J J, Jiang K, Shan L, Wang Z Y and Chen X H 2021 *Phys. Rev. X* **11** 031026
[10] Wang Z, Ma S, Zhang Y, Yang H, Zhao Z, Ou Y, Zhu Y, Ni S, Lu Z, Chen H, Jiang K, Yu L, Zhang Y, Dong X, Hu J, Gao H J, Zhao Z and Zhao Z 2021 arXiv 2104.05556
[11] Ni S L, Ma S, Zhang Y H, *et al.* 2021 *Chin. Phys. Lett.* **38** 057403
[12] Ortiz B R, Sarte P M, Kenney E M, Graf M J, Teicher S M L, Seshadri R and Wilson S D 2021 *Phys. Rev. Mater.* **5** 034801
[13] Xu H S, Yan Y J, Yin R T, Xia W, Fang S J, Chen Z Y, Li Y J, Yang W Q, Guo Y F and Feng D L 2021 *Phys. Rev. Lett.* **127** 187004
[14] Yin Q W, Tu Z J, Gong C S, Fu Y, Yan S H and Lei H C 2021 *Chin. Phys. Lett.* **38** 037403
[15] Yang S Y, Wang Y J, Ortiz B R, Liu D F, Gayles J, Derunova E, Gonzalez-Hernandez R, Smejkal L, Chen Y L, Parkin S S P, Wilson S D, Toberer E S, McQueen T and Ali M N 2020 *Sci. Adv.* **6** eabb6003
[16] Yu F H, Wu T, Wang Z Y, Lei B, Zhuo W Z, Ying J J and Chen X H 2021 *Phys. Rev. B* **104** L041103
[17] Yu L, Wang C, Zhang Y, *et al.* 2021 arXiv 2107.10714
[18] Mielke C, Das D, Yin J X, *et al.* 2022 *Nature* **602** 245
[19] Nie L P, Sun K, Ma W R, *et al.* 2022 *Nature* **604** 59
[20] Wulferding D, Lee S, Choi Y, Yin Q, Tu Z, Gong C, Lei H, Yousuf S, Song J, Lee H, Park T and Choi K Y 2022 *Phys. Rev. Res.* **4** 023215
[21] Xiang Y, Li Q, Li Y K, Xie W, Yang H, Wang Z W, Yao Y G and Wen H H 2021 *Nat. Commun.* **12** 6727
[22] Yi X W, Ma X Y, Zhang Z, Liao Z W, You J Y and Su G 2022 *Phys. Rev. B* **106** L220505
[23] Yang H, Ye Y, Zhao Z, *et al.* 2024 *Nat. Commun.* **15** 9626
[24] Werhahn D, Ortiz B R, Hay A K, Wilson S D, Seshadri R and Johrendt D 2022 *Z. Naturforsch. B* **77** 757
[25] Wang Y, Liu Y, Hao Z, *et al.* 2023 *Chin. Phys. Lett.* **40** 049901
[26] Chen X, Liu X, Xia W, Mi X, Zhong L, Yang K, Zhang L, Gan Y, Liu Y, Wang G, Wang A, Chai Y, Shen J, Yang X, Guo Y and He M 2023 *Phys. Rev. B* **107** 174510
[27] Liu B, Kuang M Q, Luo Y, *et al.* 2023 *Phys. Rev. Lett.* **131** 026701
[28] Yang J, Yi X, Zhao Z, *et al.* 2023 *Nat. Commun.* **14** 4089
[29] Wang Y, Liu Y, Hao Z, *et al.* 2023 *Chin. Phys. Lett.* **40** 037102
[30] Ortiz B R, Teicher S M L, Kautzsch L, Sarte P M, Ratcliff N, Harter J, Seshadri R and Wilson S D 2021 *Phys. Rev. X* **11** 041030
[31] Broyles C, Graf D, Yang H T, Dong X L, Gao H J and Ran S 2022 *Phys. Rev. Lett.* **129** 157001
[32] Shrestha K, Chapai R, Pokharel B K, Miertschin D, Nguyen T, Zhou X, Chung D Y, Kanatzidis M G, Mitchell J F, Welp U, Popović D, Graf D E, Lorenz B and Kwok W K 2022 *Phys. Rev. B* **105** 024508
[33] Zhang W, Wang L, Tsang C W, Liu X, Xie J, Yu W C, Lai K T and Goh S K 2022 *Phys. Rev. B* **106** 195103
[34] Fu Y, Zhao N N, Chen Z, Yin Q W, Tu Z J, Gong C S, Xi C Y, Zhu X D, Sun Y P, Liu K and Lei H C 2021 *Phys. Rev. Lett.* **127** 207002
[35] Chapai R, Leroux M, Oliviero V, Vignolles D, Bruyant N, Smylie M P, Chung D Y, Kanatzidis M G, Kwok W K, Mitchell J F and Welp U 2023 *Phys. Rev. Lett.* **130** 126401
[36] Shoenberg D 1984 *Magnetic Oscillations in Metals* (Cambridge: Cambridge Univ. Press)
[37] Alexandradinata A, Wang C, Duan W H and Glazman L 2018 *Phys. Rev. X* **8** 011027
[38] Xiao D, Chang M C and Niu Q 2010 *Rev. Mod. Phys.* **82** 1959
[39] Narayanan A, Watson M D, Blake S F, Bruyant N, Drigo L, Chen Y L, Prabhakaran D, Yan B, Felser C, Kong T, Canfield P C and Coldea A I 2015 *Phys. Rev. Lett.* **114** 117201
[40] Kresse G and Furthmüller J 1996 *Phys. Rev. B* **54** 11169
[41] Blöchl P E 1994 *Phys. Rev. B* **50** 17953
[42] Perdew J P, Burke K and Ernzerhof M 1996 *Phys. Rev. Lett.* **77** 3865
[43] Mostofi A A, Yates J R, Lee Y S, Souza I, Vanderbilt D and Marzari N 2008 *Comput. Phys. Commun.* **178** 685
[44] Rourke P M C and Julian S R 2012 *Comput. Phys. Commun.* **183** 324